

# Acoustic cloaking and mirages with flying carpets

André Diatta,<sup>1</sup> Guillaume Dupont,<sup>2</sup>  
Sébastien Guenneau,<sup>1,2</sup> and Stefan Enoch<sup>2</sup>

October 22, 2018

<sup>1</sup>Department of Mathematical Sciences, Peach Street, Liverpool L69 3BX, UK  
Email addresses: adiatta@liv.ac.uk; guenneau@liv.ac.uk

<sup>2</sup>*Institut Fresnel, UMR CNRS 6133, University of Aix-Marseille III, case 162, F13397 Marseille Cedex 20, France. Email addresses: guillaume.dupont@fresnel.fr; sebastien.guenneau@fresnel.fr; stefan.enoch@fresnel.fr;*

## Abstract

This paper extends the proposal of [Phys. Rev. Lett. 101, 203901-4 (2008)] to invisibility carpets for rigid planes and cylinders in the context of pressure acoustic waves propagating in a compressible fluid. Carpets under consideration here do not touch the ground: they levitate in mid-air (or float in mid-water), which leads to approximate cloaking for an object hidden underneath, or touching either sides of a square cylinder on, or over, the ground. The tentlike carpets attached to the sides of a square cylinder illustrate how the notion of a carpet on a wall naturally generalizes to sides of other small compact objects. We then extend the concept of flying carpets to circular cylinders and show that one can hide any type of defects under such circular carpets, and yet they still scatter waves just like a smaller cylinder on its own. Interestingly, all these carpets are described by non-singular acoustic parameters. To exemplify this important aspect, we propose a multi-layered carpet consisting of isotropic homogeneous fluids with constant bulk modulus and varying density which works over a finite range of wavelengths.

**Pacs:** 00.00, 20.00, 42.10, 42.79.-e; 02.40.-k; 41.20.-q

**Keywords:**(000.3860) Mathematical methods in physics; (260.2110) Electromagnetic theory; (160.3918) Metamaterials; (160.1190) Anisotropic optical materials; invisibility; cloak.

# 1 Introduction

There is currently a keen interest in electromagnetic metamaterials within which very unusual phenomena such as negative refraction and focussing effects involving the near field can occur [1, 2, 3, 4]. A circular cylinder coated with a negative refractive index displays anomalous resonances [5] and can even cloak a set of dipoles located in its close neighborhood [6]. The dielectric cylinder itself can be made transparent with a plasmonic coating [7].

However, cloaking of arbitrarily sized objects requires anisotropic heterogeneous media designed using transformation optics [9, 8]. The first experimental demonstration of an invisibility cloak was obtained at 8.5GHz and fueled the interest in this new field of optics [10]. Electromagnetic cloaks also allow for mirage effects [11] and their efficiency very much depend upon the smoothness of their boundaries [12]. Importantly, mathematicians have also proposed some models of cloaks, but in the context of inverse problems in tomography [13, 14] and also further explained what are the appropriate boundary conditions on the inner boundary of cloaks [15, 16]. These latter works open new vistas in acoustic cloaks, and thus attract growing attention in the physics and mathematics communities. Whereas cloaking of pressure waves in two-dimensional [18, 17] and three-dimensional [20, 21] fluids, anti-plane shear waves in cylindrical bodies [22], and flexural waves in thin-elastic plates [23, 24] is well understood by now, cloaking of in-plane coupled shear and pressure elastic waves still remains elusive [26, 25] as the Navier equations do not retain their form under geometric transforms. Such cloaks might involve (complex) pentamode materials such as proposed in [27]. However, it has been known for over ten years that coated cylinders might become neutral in the elastostatic limit [28], and this route might well be worthwhile pursuing more actively with e.g. pre-stressed coated elastic cylinders, as this would allow for a simple experimental setup.

During the same decade, some theoretical and experimental progress has been made towards a better understanding of band spectra for linear surface water waves propagating in arrays of rigid cylinders [34, 29, 30, 31, 32, 33], or over a bottom with periodically drilled holes. Focussing effect of surface water waves was also investigated by a handful of research groups in arrays of circular and square cylindrical holes [33, 35], as well as using metamaterials designed as fluid networks [36], [37]. However, a further control of surface water waves can be obtained via an alternative route, that of transforma-

tion acoustics. It has been actually demonstrated that broadband cloaking of surface water waves can be achieved with a structured cloak, with an experimental confirmation at 10 Hz[38].

In this paper, we focus our analysis on cloaking of pressure waves with carpets [39] which have recently led to experiments in the electromagnetic context [40, 41]. Here, we would like to render e.g. pipelines lying at the bottom of the sea or floating in mid-water undetectable for a boat sonar. These pipelines are considered to be infinitely long straight cylinders with a cross-section which is of circular or square shape. A pressure wave incident from above (the surface of the sea) hits the pipeline, so that the reflected wave reveals its presence to the sonar boat. We would like to show that we can hide the pipeline under a cylindrical carpet (a metafluid) so that the sonar only detects the wave reflected by the bottom of the sea.

## 2 Governing equations for pressure and transverse electric waves

For an inviscid fluid with zero shear modulus, the linearized equations of state for small amplitude perturbations from conservation of momentum, conservation of mass, and linear relationship between pressure and density are

$$\begin{aligned}\rho_0 \frac{\partial \mathbf{v}}{\partial t} &= -\nabla p \\ \frac{\partial p}{\partial t} &= -\lambda \nabla \cdot \mathbf{v}\end{aligned}\tag{1}$$

where  $p$  is the scalar pressure,  $\mathbf{v}$  is the vector fluid velocity,  $\rho_0$  is the unperturbed fluid mass density (a mass in kilograms per unit volume in meters cube), and  $\lambda$  is the fluid bulk modulus (i.e. it measures the substance's resistance to uniform compression and is defined as the pressure increase needed to cause a given relative decrease in volume, with physical unit in Pascal). This set of equations admits the usual compressional wave solutions in which fluid motion is parallel to the wavevector.

In cylindrical coordinates with  $z$  invariance, and letting the mass density be anisotropic but diagonal in these coordinates, the time harmonic acoustic equations of state simplify to (the  $\exp(-j\omega t)$  convention is used throughout)

$$\nabla \cdot (\rho_0^{-1} \nabla p) + \omega^2 \lambda^{-1} p = 0 ,\tag{2}$$

where  $\omega$  is the angular pressure wave frequency (measured in radians per unit second). Importantly, this equation is supplied with Neumann boundary conditions on the boundary of rigid defects (no flow condition).

Cummer and Schurig have shown that this equation holds for anisotropic heterogeneous fluids in cylindrical geometries [18], and they have drawn some comparisons with transverse electromagnetic waves. In the transverse electric polarization (longitudinal magnetic field parallel to the cylinder's axis):

$$\nabla \cdot (\varepsilon_r^{-1} \nabla H_z) + \omega^2 \varepsilon_0 \mu_0 H_z = 0 . \quad (3)$$

where  $H_z$  is the longitudinal (only non-zero) component of the magnetic field,  $\varepsilon_r$  is the dielectric relative permittivity,  $\varepsilon_0 \mu_0$  is the inverse of the square velocity of light in vacuum, and  $\omega$  is the angular transverse electric wave frequency (measured in radians per unit second). Importantly, this equation is supplied with Neumann boundary conditions on the boundary of infinite conducting defects.

In this paper, we look at such ‘acoustic’ models, for the case of flying carpets which are associated with geometric transforms. While we report computations for a pressure field, results apply *mutatis mutandis* to transverse electric waves making the changes of variables

$$p \longmapsto H_z , \quad \rho_0 \longmapsto \varepsilon_r , \quad \lambda^{-1} \longmapsto \varepsilon_0 \mu_0 , \quad (4)$$

in (2). However, after geometric transform, (2) will involve an anisotropic (heterogeneous) density  $\underline{\rho}$  and a varying (scalar) bulk modulus  $\lambda$ , see (12), whereas (3) would involve an anisotropic (heterogeneous) permittivity  $\underline{\varepsilon}$  and a varying (scalar) permeability  $\mu$ , see (10). It is nevertheless possible to work with a reduced set of parameters, to avoid a varying  $\lambda$  in acoustics (resp.  $\mu$  in optics), as we shall see in the last section of the paper.

### 3 From transformation optics to transformation acoustics

Let us consider a map from a co-ordinate system  $\{u, v, w\}$  to the co-ordinate system  $\{x, y, z\}$  given by the transformation characterized by  $x(u, v, w)$ ,  $y(u, v, w)$  and  $z(u, v, w)$ .

This change of co-ordinates is characterized by the transformation of the differentials through the Jacobian:

$$\begin{pmatrix} dx \\ dy \\ dz \end{pmatrix} = \mathbf{J}_{xu} \begin{pmatrix} du \\ dv \\ dw \end{pmatrix}, \text{ with } \mathbf{J}_{xu} = \frac{\partial(x, y, z)}{\partial(u, v, w)}. \quad (5)$$

In electromagnetics, this change of coordinates amounts to replacing the different materials (often homogeneous and isotropic, which corresponds to the case of scalar piecewise constant permittivity and permeability) by equivalent inhomogeneous anisotropic materials described by a transformation matrix  $\mathbf{T}$  (metric tensor). The idea underpinning acoustic invisibility [9] is that newly discovered metamaterials should enable control of the pressure waves by mimicking the heterogeneous anisotropic nature of  $\mathbf{T}$  with e.g. an anisotropic density, in a way similar to what was recently achieved with the permeability and permeability tensors in the microwave regime in the context of electromagnetism [10].

In the sequel, we propose an alternative derivation of the analogies between transformation optics and acoustics first drawn by Cummer and Schurig [18]. Our proof involves a lemma first established in [19] in the context of duality relations for the Maxwell system in checkerboards. On a geometric point of view, the matrix  $\mathbf{T} = \mathbf{J}^T \mathbf{J} / \det(\mathbf{J})$  is a representation of the metric tensor. The only thing to do in the transformed coordinates is to replace the materials (dielectric, homogeneous and isotropic) by equivalent ones which now exhibit some magnetism, which are heterogeneous (dependence upon  $u, v, w$  co-ordinates) and anisotropic. Their properties are given by [11]

$$\underline{\underline{\epsilon'}} = \epsilon_r \mathbf{T}^{-1}, \quad \text{and} \quad \underline{\underline{\mu'}} = \mathbf{T}^{-1}. \quad (6)$$

In transverse electric polarisation, the Maxwell operator in the transformed coordinates writes as

$$\nabla \times \left( \underline{\underline{\epsilon'}}^{-1} \nabla \times \mathbf{H}_l \right) - \mu_0 \epsilon_0 \omega^2 \underline{\underline{\mu'}} \mathbf{H}_l = \mathbf{0} \quad (7)$$

where  $\mathbf{H}_l = H_z(x, y) \mathbf{e}_z$ ,  $\underline{\underline{\epsilon'}}$  and  $\underline{\underline{\mu'}}$  are defined by (6).

We would like to deduce the expression of (3) in the transformed coordinates from the vector equation (7). For this, we need the following result:

**Property:** Let  $\mathbf{M}$  be a real symmetric matrix defined as follows

$$\mathbf{M} = \begin{pmatrix} m_{11} & m & 0 \\ m & m_{22} & 0 \\ 0 & 0 & m_{33} \end{pmatrix} = \begin{pmatrix} \tilde{\mathbf{M}} & 0 \\ 0 & m_{33} \end{pmatrix}. \quad (8)$$

Then we have

$$\begin{aligned} & \nabla \times \left( \mathbf{M} \nabla \times \left( u(x, y) \mathbf{e}_z \right) \right) \\ &= -\nabla \cdot \left( \tilde{\mathbf{M}}^{-1} \det(\tilde{\mathbf{M}}) \nabla u(x, y) \right) \mathbf{e}_z . \end{aligned}$$

Indeed, we note that

$$\begin{aligned} & \nabla \times \left( \mathbf{M} \nabla \times \left( u(x, y) \mathbf{e}_z \right) \right) \\ &= -\left( \frac{\partial}{\partial x} \left( m_{22} \frac{\partial u}{\partial x} - m \frac{\partial u}{\partial y} \right) \right. \\ & \quad \left. + \frac{\partial}{\partial y} \left( m_{11} \frac{\partial u}{\partial y} - m \frac{\partial u}{\partial x} \right) \right) \mathbf{e}_z \end{aligned}$$

Furthermore, let  $\mathbf{M}'$  be defined as

$$\mathbf{M}' = \begin{pmatrix} m'_{11} & m'_{12} \\ m'_{21} & m'_{22} \end{pmatrix} . \quad (9)$$

We have

$$\nabla \times \left( \mathbf{M} \nabla \times \left( u(x, y) \mathbf{e}_z \right) \right) = -\nabla \cdot \left( \mathbf{M}' \nabla u \right) \mathbf{e}_z ,$$

if and only if

$$\begin{aligned} m'_{11} \frac{\partial u}{\partial x} + m'_{12} \frac{\partial u}{\partial y} &= m_{22} \frac{\partial u}{\partial x} - m \frac{\partial u}{\partial y} \\ m'_{21} \frac{\partial u}{\partial x} + m'_{22} \frac{\partial u}{\partial y} &= m_{11} \frac{\partial u}{\partial y} - m \frac{\partial u}{\partial x} , \end{aligned}$$

which is true if  $\mathbf{M}' = \tilde{\mathbf{M}}^{-1} \det(\tilde{\mathbf{M}})$ .

Using the above property, from (7), we derive that the transformed equation associated with (3) reads

$$\nabla \cdot \underline{\underline{\epsilon}}_T'^{-1} \nabla H_z + \omega^2 \epsilon_0 \mu_0 T_{zz}^{-1} H_z = 0 , \quad (10)$$

with

$$\underline{\underline{\epsilon}}_T'^{-1} = \epsilon_r^{-1} \tilde{\mathbf{T}} / \det(\tilde{\mathbf{T}}) . \quad (11)$$

Here,  $\tilde{\mathbf{T}}$  denotes the upper diagonal part of the transformation matrix  $\mathbf{T}$  and  $T_{zz}$  its third diagonal entry.

Invoking the one-to-one correspondence (4), we infer that the transformed equation associated with (2) reads

$$\nabla \cdot \underline{\underline{\rho}}_T'^{-1} \nabla p + \omega^2 \lambda^{-1} T_{zz}^{-1} p = 0, \quad (12)$$

with

$$\underline{\underline{\rho}}_T'^{-1} = \rho_0^{-1} \tilde{\mathbf{T}} / \det(\tilde{\mathbf{T}}). \quad (13)$$

In the sequel we will also consider a compound transformation. Let us consider three coordinate systems  $\{u, v, w\}$ ,  $\{X, Y, Z\}$ , and  $\{x, y, z\}$  (possibly on different regions of spaces). The two successive changes of coordinates are given by the Jacobian matrices  $\mathbf{J}_{xX}$  and  $\mathbf{J}_{Xu}$  so that

$$\mathbf{J}_{xu} = \mathbf{J}_{xX} \mathbf{J}_{Xu}. \quad (14)$$

This rule naturally applies for an arbitrary number of coordinate systems.

## 4 Flying carpets over a flat ground plane

This section is dedicated to the study of carpets levitating above a ground plane, that conceal to certain extent any object placed anywhere underneath them from plane waves incident from above. The construction of the carpet is a generalization of those considered in [39] to carpets flying over ground planes or located on either sides of rectangular objects, as shown in Fig. 1 with certain altitude  $y = y_0$ . In the context of pressure waves, this corresponds for instance to the physical situation of a carpet which flies in mid-air if  $y = 0$  is the altitude of the ground, or a carpet which floats in mid-waters if  $y = 0$  stands for the bottom of the sea. This formalism allows us to study carpets which are either flying/floating on their own, or which are touching a cylindrical object on the ground or in mid-air/water.

### 4.1 The construction of carpets over horizontal planes

When the carpet is made on the  $y$ -axis (we call it a carpet flying above the  $x$ -axis), we consider a transformation mapping the region enclosed between

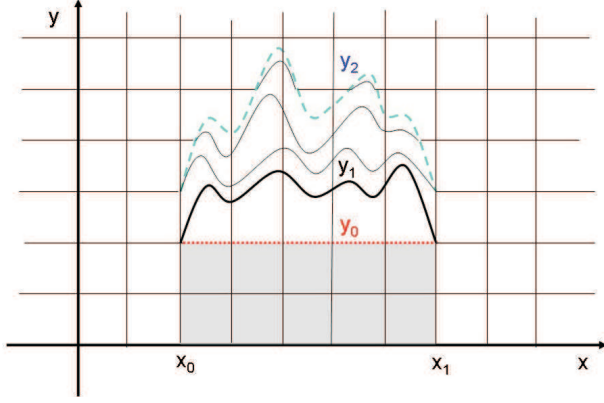


Figure 1: (Color online) Construction of a carpet above the  $x$ -axis. The transformation (15) shrinks the region between the two curves  $y = \mathbf{y}_0$  (dotted red) and  $y = y_2(x)$  (dashed blue) and two vertical segments  $x = x_0$  and  $x = x_1$  into the region between the curves  $y = y_1(x)$  (solid black) and  $y = y_2(x)$  (dashed blue) and the vertical segments  $x = x_0$  and  $x = x_1$  (carpet). The curvilinear metric inside the carpet is described by the transformation matrix  $\mathbf{T}$ , see (19), corresponding to density and bulk modulus of the metafluid given by (6). The grey rectangle can be either filled with air/ambient fluid (flying/floating carpet) or be replaced by a rigid cylinder.

two curves  $(x, y_0)$  and  $(x, y_2(x))$  to the one comprised between  $(x, y_1(x))$  and  $(x, y_2(x))$  as in Fig. 1, where  $(x, y_0)$  is mapped on  $(x, y_1(x))$  and  $(x, y_2(x))$  is fixed point-wise, of the form

$$\begin{cases} x' = x \\ y' = \alpha(x)y + \beta(x) \text{ with } \alpha = \frac{y_2 - y_1}{y_2 - y_0} \text{ and } \beta = \frac{y_1 - y_0}{y_2 - y_0} y_2 \\ z' = z \end{cases} \quad (15)$$

So the inverse of this transformation is given by

$$\begin{cases} x = x' \\ y = \frac{y' - \beta(x')}{\alpha(x')} \\ z = z' \end{cases} \quad (16)$$

The above transformation (16) has the following Jacobian matrix

$$\mathbf{J}_{xx'} = \frac{\partial(x, y, z)}{\partial(x', y', z')} = \begin{pmatrix} 1 & 0 & 0 \\ g & \frac{1}{\alpha} & 0 \\ 0 & 0 & 1 \end{pmatrix}. \quad (17)$$



in which we have set

$$\begin{aligned}
g &:= \frac{\partial y}{\partial x'} = \frac{1}{\alpha^2} \left( -\alpha \frac{d\beta}{dx'} - (y' - \beta) \frac{d\alpha}{dx'} \right) \\
&= -\frac{(y_2 - y')(y_2 - y_0)}{(y_2 - y_1)^2} \frac{dy_1}{dx} \\
&+ \frac{(y_1 - y')(y_1 - y_0)}{(y_2 - y_1)^2} \frac{dy_2}{dx}.
\end{aligned} \tag{18}$$

Hence we get

$$\mathbf{T}^{-1} = \mathbf{J}_{xx'}^{-1} \mathbf{J}_{xx'}^{-T} \det(\mathbf{J}_{xx'}) = \begin{pmatrix} \frac{1}{\alpha} & -g & 0 \\ -g & (1 + g^2)\alpha & 0 \\ 0 & 0 & \frac{1}{\alpha} \end{pmatrix}. \tag{19}$$

## 4.2 Analysis of the metamaterial properties

Let us now look at an interesting feature of the invisibility carpet. The eigenvalues of  $\mathbf{T}^{-1}$  are given by:

$$\begin{aligned}
i = 1, 2 : \lambda_i &= \frac{1}{2\alpha} \left( 1 + \alpha^2 + g^2\alpha^2 + (-1)^i \sqrt{-4\alpha^2 + (1 + \alpha^2 + g^2\alpha^2)^2} \right), \\
\lambda_3 &= \frac{1}{\alpha}.
\end{aligned} \tag{20}$$

We note that  $\lambda_i$ ,  $i = 1, 2$ , and  $\lambda_3$  are strictly positive functions as obviously  $1 + \alpha^2 + g^2\alpha^2 > \sqrt{-4\alpha^2 + (1 + \alpha^2 + g^2\alpha^2)^2}$  and also  $\alpha > 0$ . This establishes that  $\mathbf{T}^{-1}$  is not a singular matrix for a two-dimensional carpet even in the case of curved ground planes, which is one of the main advantages of carpets over cloaks [39]. The broadband nature of such carpets remains to be investigated when one tries to mimic their ideal material parameters with structured media.

The carpets in Fig. 2 and 3 are made of a semi-circle  $y = y_2(x)$  as an outer curve and a semi-ellipse  $y = y_1(x)$  as its inner curve, both centered at  $(a_0, b_1)$  with

$$\begin{aligned}
y_0 &= b_0, \quad y_1(x) = b_1 + \left(1 - \frac{k_0}{r_0}\right) \sqrt{r_0^2 - (x - a_0)^2}, \\
y_2(x) &= b_1 + \sqrt{r_0^2 - (x - a_0)^2}.
\end{aligned} \tag{21}$$

Plugging the numerical values  $r_0 := 0.2, k_0 = 0.1, a_0 = 0$  in, one gets

$$g = \frac{(5x(50b_1(b_0 - b_1) + 1 - 25x^2 + 50y(b_1 - b_0)))}{(1 - 25x^2)^{\frac{3}{2}}},$$

where  $b_0$  is the  $y$ -coordinate of the ground (typically, the ground can be taken as  $y = 0$ , so that  $b_0 = 0$ ) and  $b_1$  is the height, measured on the  $y$ -axis from the origin, at which the carpet is flying.

### 4.3 The construction of carpets over vertical planes

We note that for a carpet flying above the  $y$ -axis, if we consider the transformation mapping the region enclosed between two curves  $(x_0(y), y)$  and  $(x_2(y), y)$  to the one comprised between  $(x_1(y), y)$  and  $(x_2(y), y)$  as in Fig. 1, where again  $(x_0(y), y)$  is mapped on  $(x_1(y), y)$  and  $(x_2(y), y)$  is fixed point-wise, that is, if

$$\begin{cases} x' = \alpha(y)x + \beta(y) & \text{with } \alpha = \frac{x_2 - x_1}{x_2 - x_0} \text{ and } \beta = \frac{x_1 - x_0}{x_2 - x_0}x_2 \\ y' = y \\ z' = z \end{cases}$$

then the Jacobian of the inverse transformation now reads

$$\mathbf{J}_{xx'} = \frac{\partial(x, y, z)}{\partial(x', y', z')} = \begin{pmatrix} \frac{1}{\alpha} & h & 0 \\ 0 & 1 & 0 \\ 0 & 0 & 1 \end{pmatrix} \quad (22)$$

where  $h$  is defined as

$$\begin{aligned} h &:= \frac{\partial x}{\partial y'} = \frac{1}{\alpha^2} \left( -\alpha \frac{d\beta}{dy'} - (x' - \beta) \frac{d\alpha}{dy'} \right) \\ &= -\frac{(x_2 - x')(x_2 - x_0)}{(x_2 - x_1)^2} \frac{dx_1}{dy} \\ &+ \frac{(x_1 - x')(x_1 - x_0)}{(x_2 - x_1)^2} \frac{dx_2}{dy}. \end{aligned} \quad (23)$$

and hence we get

$$\mathbf{T}^{-1} = \begin{pmatrix} (1 + h^2)\alpha & -h & 0 \\ -h & \frac{1}{\alpha} & 0 \\ 0 & 0 & \frac{1}{\alpha} \end{pmatrix}. \quad (24)$$

The same analysis as in Section 4.2 literally applies here, as well.

## 4.4 Numerical results for a carpet over a plane

We first look at the case of a pressure plane wave incident upon a flat rigid ground plane (Neumann boundary conditions) and a carpet above it. The inner boundary of the carpet is rigid (Neumann boundary conditions). We report these results in Figure 2 where we can see that the altitude  $y' = 0.9$  leads to less scattering than the other two flying carpets. Of course, the carpet attached to the ground plane leads to perfect invisibility.

We then look at the case of the rigid ground plane with a rigid circular obstacle on top of it. Some Neumann boundary conditions are set on the ground plane, the inner boundary of the carpet and the rigid obstacle. Once again, we can see in Figure 3 that the altitude  $y' = 0.9$  for the flying carpet is the optimal one.

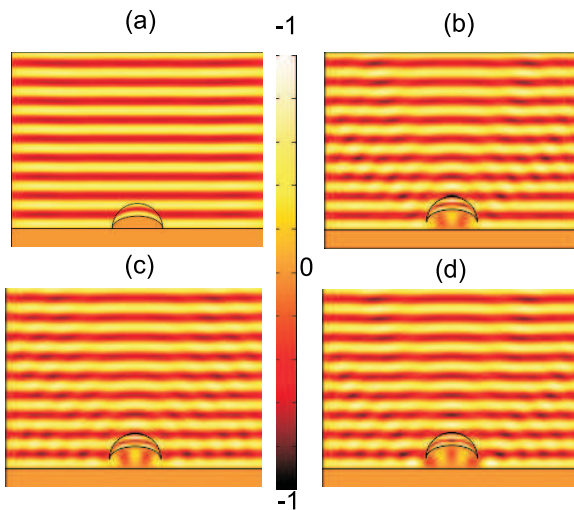


Figure 2: (Color online) 2D plot of the real part of the total pressure field  $\Re(p)$ : Scattering by a pressure plane wave of wavelength 0.15 incident from the top on a flat ground plane with a carpet above it, here  $y_1(x) = b_1 + 1/2\sqrt{0.04 - x^2}$  and  $y_2(x) = b_1 + \sqrt{0.04 - x^2}$ . (a) carpet touching the ground, (b) carpet flying at altitude  $b_1 = 0.7$ , (c) at  $b_1 = 0.9$  and (d) at  $b_1 = 1$ . The optimal altitude (for a flying carpet)  $b_1 = 0.9$  is noted.

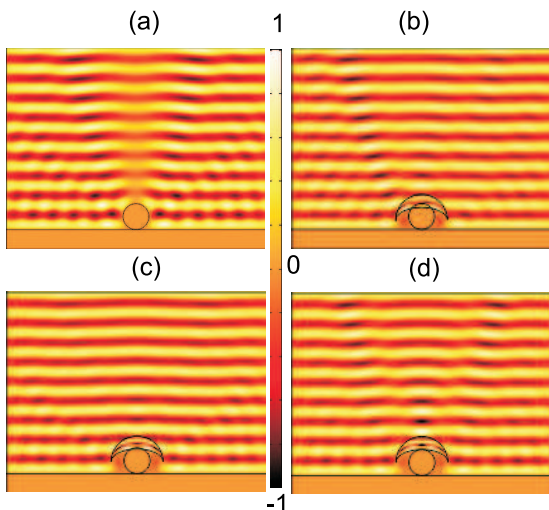


Figure 3: (Color online) 2D plot of the real part of the total pressure field  $\Re(p)$ : Scattering by a pressure plane wave of wavelength 0.15 incident from above on a circular object of radius  $r = 0.6$  lying on a flat ground plane; (a) obstacle without carpet, (b) with a carpet flying at altitude  $b_1 = 0.7$ , (c) at  $b_1 = 0.9$  and (d) at  $b_1 = 1$ . The optimal altitude  $b_1 = 0.9$  is noted.

#### 4.5 Numerical results for a carpet over a square cylinder over a plane

In this paragraph, we would like to render a pipeline lying on the bottom of the sea or floating in mid-water undetectable for a boat with a sonar at rest just above it on the surface of the sea. However, instead of reducing its scattering cross-section like in acoustic cloaks, we rather mimic that of another obstacle, say a square rigid cylinder.

In Fig. 4, we plot the total field when the pressure wave of wavelength 0.15 is incident from above on a rigid square cylinder of sidelength 0.4. In panel (a) the obstacle touches the ground (e.g. bottom of the sea) at  $y = -1.26$  and is centered about  $x = 0$ . In panel (b), it has three carpets shaped as tents attached to its sides. The construction of the carpets is as follows: The right-most tent is defined by  $x_0 = 0.2$ ,  $x_1(y) = -y - 0.66$ ,  $x_2(y) = -y - 0.56$  (upper part) and  $x_1(y) = y + 1.46$ ,  $x_2(y) = y + 1.56$  (lower part). The left-most tent is defined by  $x_0 = -0.2$ ,  $x_1(y) = -y - 1.46$ ,  $x_2(y) = -y - 1.56$  (lower part), and  $x_1(y) = y + 0.66$ ,  $x_2(y) = y + 0.56$  (upper part). The

pressure and bulk modulus of these left-most and right-most tents is deduced from the expression of the transformation matrix for vertical walls, see (24). Finally, the uppermost tent is defined by  $y_0 = -0.86$ ,  $y_1(x) = -x - 0.66$ ,  $y_2(x) = -x - 0.56$  (right part) and  $y_1(x) = x - 0.66$ ,  $y_2(x) = x - 0.56$  (to the left). Here, we use the expression of the transformation matrix for horizontal walls, see (19).

We now look at the case of a floating rigid square cylinder of sidelength 0.4 in mid-water (e.g. a pipeline). In panel (c), the obstacle is flying on its own. In panel (d), it has three tentlike carpets on its sides and yet still scatters the incoming wave as in (c). The construction of the carpets in panel (d) is as follows: The right-most tent is defined by  $x_0 = 0.2$ ,  $x_1(y) = -y + 0.4$ ,  $x_2(y) = -y + 0.5$  (upper part) and  $x_1(y) = y + 0.4$ ,  $x_2(y) = y + 0.5$  (lower part). Similarly, the left-most tent is defined by  $x_0 = -0.2$ ,  $x_1(y) = -y - 0.4$ ,  $x_2(y) = -y - 0.5$  (lower part) and  $x_1(y) = y - 0.4$ ,  $x_2(y) = y - 0.5$  (upper part). Finally, the uppermost tent is defined by  $y_0 = 0.2$ ,  $y_1(x) = -x + 0.4$ ,  $y_2(x) = -x + 0.5$  (right) and  $y_1(x) = x + 0.4$ ,  $y_2(x) = x + 0.5$  (left).

We note that while forward and backward scattering in panels (b) and (d) are not negligible (as would be the case for acoustic cloaks), these are instantly recognizable as that of a square obstacle on the ground (panel a) or floating in mid-water (panel c). The next question to address is whether such a generalized cloaking works at other incidences.

## 4.6 Numerical results for a carpet over a square cylinder over a plane in grazing incidence

We now look at the case of grazing incidence, keeping otherwise the same configuration as in Fig. 4. We note that the total field for the square obstacle is exactly the same with and without the three carpets, which is a further evidence that carpets allow for multi-incidence cloaking. Of course, one can hide any object (e.g. a semi-disc) under the carpets in panel (b) and this will scatter as a square. However, in the case of a flying object, it is required that the lower boundary of the hidden object be flat (e.g. a semi-disc) in order to mimic the diffraction pattern associated with a square obstacle.

Taking into account that it should be possible to design broadband carpets as their material parameters are non-singular, our numerics suggest that carpets are thus a very interesting alternative to invisibility cloaks. They can either reduce the scattering cross section of a rigid object or mimic that of

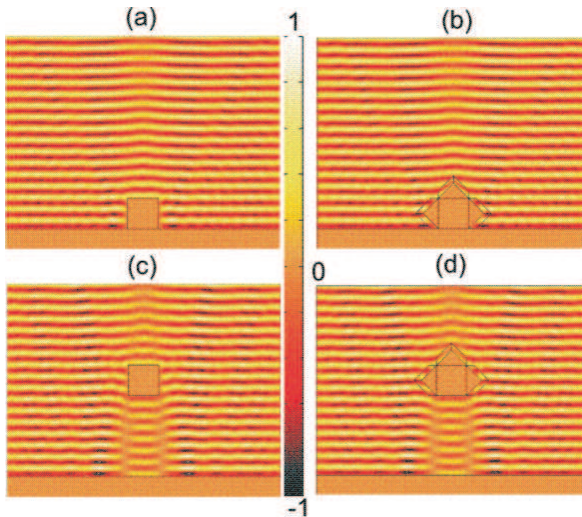


Figure 4: (Color online) 2D plot of the real part of the total pressure field  $\Re(p)$ : Scattering by a pressure plane wave of wavelength 0.15 incident from above on a rigid square cylinder of sidelength  $d = 0.4$  lying on a flat ground plane on its own (a); with three (tentlike) carpets on its sides (b); flying over the ground plane on its own (c); with three (tentlike) carpets on its sides (d).

another rigid object.

Finally, we should emphasize that we numerically checked that our proposal for generalized carpets works fine for a pressure plane wave incident on the square at any angles ranging from normal to grazing incidence. This should not come as a surprise as the same holds true in the original proposal by Li and Pendry [39].

## 5 Flying carpets surrounding a circular cylinder over a plane

We propose in this section to design a carpet which geometrically looks like Pendry's cylindrical cloak [9], but in fact, it scatters any incoming plane wave just like a rigid cylinder of smaller radius  $R_0$ . The radius of such an effective rigid cylinder can be of any size smaller than that of the coated region. Such a carpet acts in a way similar to the invisibility cloaks proposed by Greenleaf et al. and Kohn et al. which are based upon the blow up

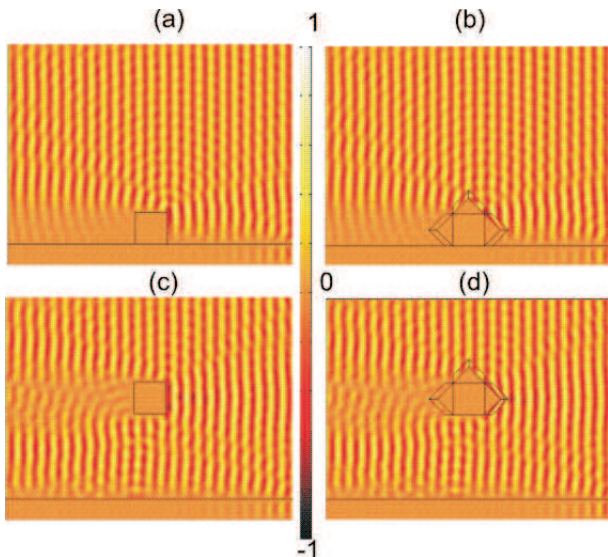


Figure 5: (Color online) 2D plot of the real part of the total pressure field  $\Re(p)$ : Scattering by a pressure plane wave of wavelength 0.15 incident from the right (grazing incidence) on a rigid square cylinder of sidelength  $d = 0.4$  lying on a flat ground plane on its own (a); with three tentlike carpets on its sides (b); flying over the ground plane on its own (c); with three tentlike carpets on its sides (d).

of a small ball (of radius  $\eta \ll 1$ ) rather than a point, thereby leading to approximate invisibility. However, in our case, the radius of this ball (a disc in 2D) is finite, and our claim is that the carpet mimics the electromagnetic response of the rigid circular cylinder, just like previous carpets did for planes. The circular carpet actually plays the opposite role to the super-scatterer of Nicorovici, McPhedran and Milton whereby a cylinder surrounded by a coating of negative refractive index material scatters as a cylinder of diameter larger than the coating itself [5].

However, whether this coated region is completely empty (e.g. Fig 7(b)) or many objects are hidden inside it (see e.g. Fig. 7(d) where the small cylinder of radius  $R_0$  has actually been put back inside the carpet, along with other objects), such a carpet produces a mirage effect that tricks an external observer into believing that this whole region is just the small rigid cylinder.

## 5.1 The construction of circular carpets

The carpet consists of a cylindrical region  $C(\underline{0}, R_1)$  of radius  $R_1$  to be coated and the coating itself which is the space between an inner cylinder of radius  $R_1$  and an outer one of radius  $R_2 > R_1$ . As above, the material properties of this coating will be deduced by pullback, via a transformation that fixes angles just like in [9]. The transformation in [9] is indeed the particular case, of the one under consideration here, associated with the value  $R_0 = 0$  of the radius of an imaginary small cylinder as explained below.

The carpet constructed below is a generalization of the flying carpet studied in the previous section. The geometric transformation we consider here, is a smooth diffeomorphism of the closure of the outside  $\mathbb{R}^3 \setminus C(\underline{0}, R_0)$  of a solid cylinder  $C(\underline{0}, R_0)$  of radius  $R_0$ , where  $R_0 < R_1$ . It coincides with the identity map outside the solid cylinder  $C(\underline{0}, R_2)$ , fixing its boundary pointwise, but now maps the region  $\mathcal{A}(R_0, R_2)$  between the two coaxial cylinders of respective radii  $R_0$  and  $R_2$  into the space  $\mathcal{A}(R_1, R_2)$  between the cylinders of radii  $R_1$  and  $R_2$ , as in Fig. 6. More precisely, in  $\mathcal{A}(R_0, R_2)$  this geometric transformation can be expressed as

$$\begin{cases} r' = R_1 + \alpha(r - R_0) & \text{with } \alpha = \frac{R_2 - R_1}{R_2 - R_0} \\ \theta' = \theta \\ z' = z \end{cases} \quad (25)$$

with inverse

$$\begin{cases} r = R_0 + \frac{1}{\alpha}(r' - R_1) \\ \theta = \theta' \\ z = z' \end{cases}$$

The Jacobian  $\mathbf{J}_{rr'}$  of the latter is

$$\mathbf{J}_{rr'} = \frac{\partial(r, \theta, z)}{\partial(r', \theta', z')} = \text{diag}\left(\frac{1}{\alpha}, 1, 1\right). \quad (26)$$

Let us denote by  $\mathbf{J}_{xr}$  the Jacobian of the change  $(r, \theta, z) \mapsto (x, y, z)$  from Cartesian to polar coordinates and  $\mathbf{J}_{rx} := \mathbf{J}_{xr}^{-1}$ . The Jacobian  $\mathbf{J}_{xx'}$  of the above transformation in Cartesian coordinates  $(x', y', z') \mapsto (x, y, z)$  is obtained by applying the chain rule (14) to get  $\mathbf{J}_{xx'} = \mathbf{J}_{xr}\mathbf{J}_{rr'}\mathbf{J}_{r'x'}$ , so that the tensor



$\mathbf{T}^{-1} = \mathbf{J}_{xx'}^{-1} \mathbf{J}_{xx'}^{-T} \det(\mathbf{J}_{xx'})$  reads

$$\begin{aligned} \mathbf{T}^{-1} &= \begin{pmatrix} \frac{1+(m^2-1)\cos^2(\theta)}{m} & \frac{(m^2-1)\sin(\theta)\cos(\theta)}{m} & 0 \\ \frac{(m^2-1)\sin(\theta)\cos(\theta)}{m} & \frac{m^2+(1-m^2)\cos^2(\theta)}{m} & 0 \\ 0 & 0 & \frac{m}{\alpha^2} \end{pmatrix} \\ &= R(\theta) \text{diag}\left(m, \frac{1}{m}, \frac{m}{\alpha^2}\right) R(-\theta), \end{aligned} \quad (27)$$

where  $\mathbf{R}(\theta) = \begin{pmatrix} \cos(\theta) & -\sin(\theta) & 0 \\ \sin(\theta) & \cos(\theta) & 0 \\ 0 & 0 & 1 \end{pmatrix}$  is the matrix of the rotation with angle  $\theta$  in the  $xy$ -plane and  $m = \frac{\alpha r}{r'} = 1 - \frac{R_1 - R_0}{(R_2 - R_0)} \frac{R_2}{r'}$ .

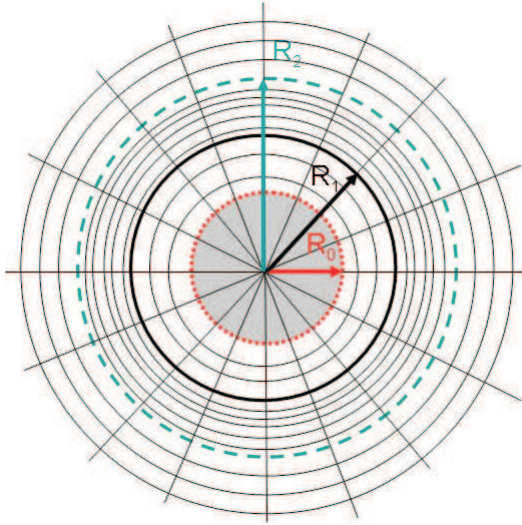


Figure 6: (Color online) Construction of a circular carpet of inner radius  $R_1$  (solid dark) and outer radius  $R_2$  (dashed blue) from cylinder  $\mathcal{S}(\underline{0}, R_0)$  of smaller radius  $R_0$  (dotted red). The transformation (25) shrinks the whole hollow cylindrical region  $\mathcal{A}(R_0, R_2)$  of inner radius  $R_0$  and outer radius  $R_2$  into its subset  $\mathcal{A}(R_1, R_2)$ , the cylinder  $\mathcal{S}(\underline{0}, R_0)$  being stretched to  $\mathcal{S}(\underline{0}, R_1)$  whereas  $\mathcal{S}(\underline{0}, R_2)$  is fixed point-wise. Such a carpet, a metafluid with bulk modulus and density given by (27) and (6), scatters pressure waves as the rigid cylinder  $\mathcal{S}(\underline{0}, R_0)$ .

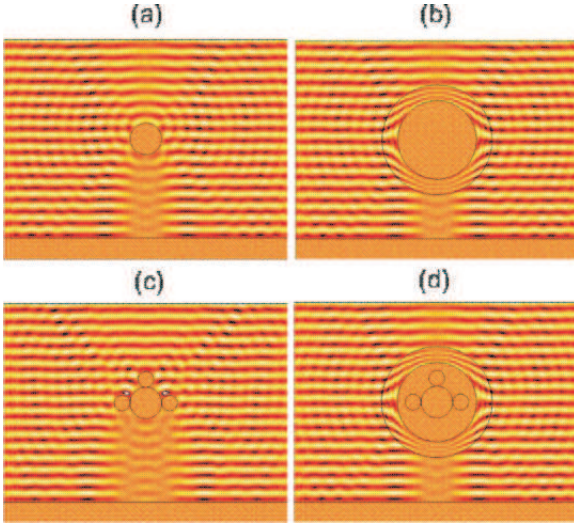


Figure 7: (Color online) 2D plot of the real part of the total pressure field  $\Re(p)$ : Scattering by a plane wave of wavelength 0.15 incident from above on a flat ground plane and (a) a circular object of radius  $R_0 = 0.2$  flying at altitude on its own; (b) an empty cylindrical region of radius  $R_1 = 0.5$ , the "coated" region, surrounded by a carpet of inner radius  $R_1$  and outer radius  $R_2 = 0.7$ . This hollow cylindrical carpet is designed to behave exactly like the object in (a) alone, irrespective of the form of any other additional object that may be enclosed inside; (c) same object as in (a) with now three additional small rigid cylinders touching it. The scattering is clearly different from that in (a); (d) now the three objects in as (c) have been hidden inside the carpet (b) and yet an outer observer will not be able to tell the scattering in (a) and in (d) apart.

## 5.2 Analysis of the metamaterial properties

The tensor  $\mathbf{T}^{-1}$  diagonalizes as  $\text{diag}(m, \frac{1}{m}, \frac{m}{\alpha^2})$  where  $m = 1 - \frac{R_1 - R_0}{(R_2 - R_0)} \frac{R_2}{r'}$  is bounded from below and above as it satisfies  $0 < \alpha \frac{R_0}{R_1} \leq m \leq \alpha$ . This means that the material parameters are not singular, unlike the cloaking case as in [9].

Obviously, one realizes that, when  $R_0$  tends to zero, one recovers the case in [9] where the material properties are no longer bounded, but one of them tends to zero whilst another one recedes to infinity, as we approach the inner boundary of the coated region, see also [14].

### 5.3 Mirage effect for a cylinder surrounded by a carpet

We report the results of our simulations in Fig. 7 for a circular pipeline which is floating in mid-water, see panel (a). We then replace this pipeline by a circular carpet, see panel (b), which reflects a pressure plane wave from above at wavelength 0.5 in exactly the same way. When we add three small pipelines to the original one, see panel (c), the reflected field is obviously much different. However, when we surround the four pipelines by the circular carpet, see panel (d), the reflected wave is that of the original pipeline. Such a mirage effect, whereby a rigid obstacle hides other ones in its neighborhood, can thus be used for 'sonar illusions'. For instance, an oil pipeline might reflect pressure waves like a coral barrier so that a sonar boat won't catch its presence. Unlike for earlier proposals of approximate cloaks [13, 14] scattering waves like a small highly conducting object, we emphasize here that we start the construction of the circular carpet by a finite size disc.

## 6 Multilayered circular carpet for broadband mirage effect

### 6.1 Reduced material parameters for circular carpets

We now want to simplify the expression of the inverse of the transformation matrix  $\mathbf{T}$  in order to avoid a varying (scalar) density (resp. permeability in optics). For this, we introduce the reduced matrix  $\mathbf{T}_{red}^{-1} = \text{diag}(\alpha, \frac{\alpha}{m^2}, \frac{1}{\alpha})$  which amounts to multiplying  $\mathbf{T}^{-1}$  in (27) by  $\alpha/m$ . We deduce from (2) the transformed governing equation for pressure waves in reduced coordinates:

$$\nabla_{r,\theta} \cdot \text{diag}\left(\frac{1}{\alpha}, \frac{m^2}{\alpha}\right) \nabla_{r,\theta} p + \omega^2 \lambda^{-1} \alpha p = 0, \quad (28)$$

and similarly for transverse electric waves using (3):

$$\nabla_{r,\theta} \cdot \text{diag}\left(\frac{1}{\alpha}, \frac{m^2}{\alpha}\right) \nabla_{r,\theta} H_z + \omega^2 \epsilon_0 \mu_0 \alpha H_z = 0, \quad (29)$$

where  $m = 1 - \frac{R_1 - R_0}{(R_2 - R_0)} \frac{R_2}{r'}$  and  $\alpha = \frac{R_2 - R_1}{R_2 - R_0}$ .

## 6.2 Homogenized governing equations for optics and acoustics

To illustrate our paper with a practical example, we finally choose to design a circular carpet using 40 layers of isotropic homogeneous fluids. These fluids have constant bulk modulus and varying density. We report these computations in figure 8.

It is indeed well known that the homogenized acoustic equation for such a configuration takes the following form:

$$\nabla_{r,\theta} \cdot (\underline{\underline{\rho}}_0^{-1} \underline{\underline{\rho}}^{-1} \nabla_{r,\theta} H_z) + \omega^2 \langle \lambda^{-1} \rangle p = 0, \quad (30)$$

where  $\langle \lambda^{-1} \rangle = \int_0^1 \lambda^{-1}(r) dr$  and with  $\underline{\underline{\rho}}$  a homogenized rank-2 diagonal tensor (an anisotropic density)  $\underline{\underline{\rho}} = \text{Diag}(\rho_r, \rho_\theta)$  given by

$$\underline{\underline{\rho}} = \text{Diag}(\langle \rho^{-1} \rangle^{-1}, \langle \rho \rangle). \quad (31)$$

We note that if the cloak consists of an alternation of two homogeneous isotropic layers of fluids of thicknesses  $d_A$  and  $d_B$ , with bulk moduli  $\lambda_A$  and  $\lambda_B$  and densities  $\rho_A$  and  $\rho_B$ , we have

$$\begin{aligned} \frac{1}{\rho_r} &= \frac{1}{1+\eta} \left( \frac{1}{\rho_A} + \frac{\eta}{\rho_B} \right), \\ \rho_\theta &= \frac{\rho_A + \eta \rho_B}{1+\eta}, \quad \langle \lambda^{-1} \rangle = \frac{1}{1+\eta} \left( \frac{1}{\lambda_A} + \frac{\eta}{\lambda_B} \right), \end{aligned}$$

where  $\eta = d_B/d_A$  is the ratio of thicknesses for layers  $A$  and  $B$  and  $d_A + d_B = 1$ .

Using the change of variables

$$\nabla_{r,\theta} \cdot (\underline{\underline{\varepsilon}}_r^{-1} \underline{\underline{\varepsilon}}^{-1} \nabla_{r,\theta} p) + \varepsilon_0 \mu_0 \omega^2 H_z = 0, \quad (32)$$

where  $\underline{\underline{\varepsilon}}$  is a homogenized rank-2 diagonal tensor (an anisotropic permittivity)  $\underline{\underline{\varepsilon}} = \text{Diag}(\varepsilon_r, \varepsilon_\theta)$  given by

$$\underline{\underline{\varepsilon}} = \text{Diag}(\langle \varepsilon^{-1} \rangle^{-1}, \langle \varepsilon \rangle). \quad (33)$$

### 6.3 Acoustic paradigm: Reduced scattering with larger scatterer

The acoustic parameters of the proposed layered circular carpet are therefore characterized by a spatially varying scalar bulk modulus  $\rho$  and a spatially varying rank 2 density tensor  $\underline{\underline{\rho}}$  given by (33). We can further simplify the problem by choosing reduced acoustic parameters, so that the bulk modulus  $\lambda$  is now constant, and all the variation is reported on the density, see figure 8. More precisely,  $\rho_A$  varies in the range  $[0.1890; 0.5493]$  and  $\rho_B$  varies in the range  $[1.7987; 2.1472]$ . We checked that this carpet is broadband as it works over the range of wavelengths  $\lambda \in [0.2, 1.4286]$ , see Fig. 8 and Fig. 9: a multilayered carpet of radius 1 surrounding a rigid obstacle of radius 0.32 scatters waves just like a rigid obstacle of radius  $R_0 = 0.2$ . We note that the lower bound for the range of working wavelengths corresponds to the rigid obstacle we want to mimic.

## 7 Conclusion

In this paper, we have proposed some models of flying carpets which levitate (or float) in mid-air (or mid-water). Such cloaks can be built from acoustic metafluids: as explained by Pendry and Li in a recent work, one can for instance emulate required anisotropic density and heterogeneous bulk modulus with arrays of rigid plates with a hemispherical sack of gaz attached to them [42]. But other designs proposed by Torrent and Sanchez-Dehesa would work equally well [17]. However, such flying carpets lead to some approximate cloaking as they do not touch the ground (the inner boundary of the carpet in the original design of Pendry and Li is attached to the ground [39]. Interestingly, other authors also looked at quasi-cloaking with simplified carpets [43]. We have also explained how one can hide an object located in the close neighborhood of a rigid circular cylinder, which in some sense can be classified as an external cloaking whereby a large scatterer hides smaller ones located nearby. Such an ostrich effect (which buries its head in the sand) has already been observed in the context of dipoles and even finite size obstacles located closeby a cylindrical perfect lens which displays anomalous resonances [6, 44]. However, here the coating does not contain any negatively refracting material, and this is an anisotropy-led rather than plasmonic-type cloaking mechanism. Actually, it is possible to use complementary media to

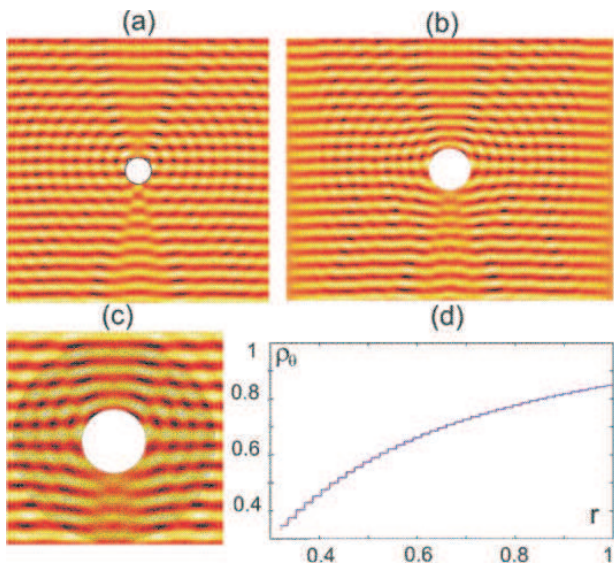


Figure 8: (Color online) 2D plot of the real part of the total pressure field  $\Re(p)$ : Scattering by a plane wave of wavelength 0.2 incident from above on a flat ground plane and (a) a circular object of radius  $R_0 = 0.2$  flying at altitude on its own; (b) an empty cylindrical region of radius  $R_1 = 0.32$ , the "coated" region consisting of 40 layers of isotropic homogeneous fluid, see closer view in (c), of constant bulk modulus and density  $\rho$ , given in (d), surrounded by a carpet of inner radius  $R_1$  and outer radius  $R_2 = 1$ . The red curves represents the variation of  $\rho_\theta = m^2/\alpha$  with respect to  $r \in [0.32; 1]$ . The piecewise constant blue curve is a staircase approximation of the red curve, considering an alternation of 40 layers of density  $\rho_A \in [0.1890; 0.5493]$  and  $\rho_B \in [1.7987; 2.1472]$  using the homogenized formula (33).

cloak finite size objects (rather than only dipoles) at a finite distance [45].

We have discussed some applications, with the sonar boats or radars cases as typical examples. Another possible application would be protecting parabolic antennas from the negative impact of their 'supporting cable'. The feasibility of such carpets is demonstrated using a homogenization approach enabling us to design a multi-layered acoustic metafluid leading to a mirage effect over a finite range of wavelengths. We note that the route towards anamorphism discussed in this paper is very different from the proposal of Nicolet et al. [46] whereby an anisotropic heterogeneous object is placed within the coating of a singular cloak to mimic the scattering of another

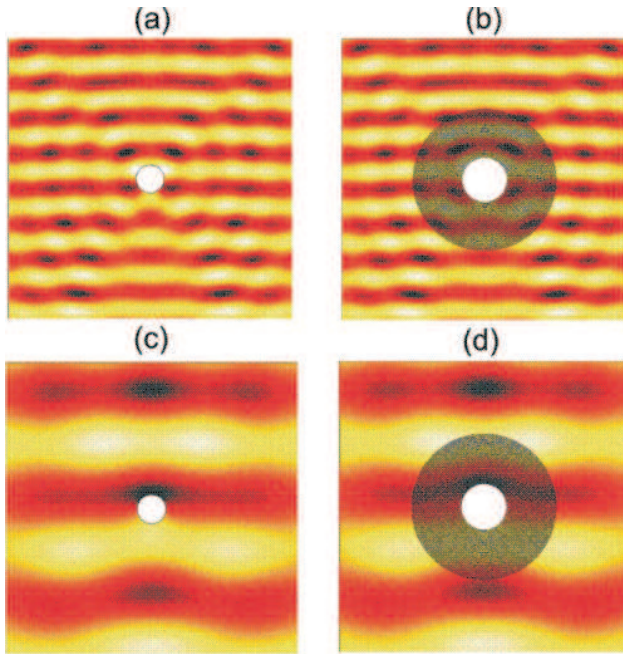


Figure 9: (Color online) 2D plot of the real part of the total pressure field  $\Re(p)$  for the same geometric and acoustic parameters as in Fig. 8; Scattering by a plane wave of wavelength 0.5 (a-b) and 1.4286 (c-d), incident from above.

object.

Moreover, all computations hold for electromagnetic carpets built with heterogeneous anisotropic permittivity and scalar permittivity, which could be emulated using tapered waveguides as in [47]. We therefore believe that the designs we proposed in this paper might foster experimental efforts in approximate cloaking for both acoustic and electromagnetic waves.

## Acknowledgements

AD and SG acknowledge funding from the Engineering and Physical Sciences Research Council grant EPF/027125/1.

## References

- [1] V.G. Veselago 1967 Usp. Fiz. Nauk 92 517. V.G. Veselago, Sov. Phys.Usp. 10 509 (1968)
- [2] J.B. Pendry, Phys. Rev. Lett. 86, 3966-3969 (2000).
- [3] Smith, D.R., Padilla, W.J., Vier, V.C., Nemat-Nasser, S.C., Schultz, S., Phys. Rev. Lett. 84, 4184 (2000)
- [4] S.A. Ramakrishna, Rep. Prog. Phys. 68 449 (2005).
- [5] N.A. Nicorovici, R.C. McPhedran, G.W. Milton, Phys. Rev. B 49, 8479-8482 (1994).
- [6] G. Milton and N.A. Nicorovici, Proc. Roy. Soc. Lond. A **462** 3027 (2006).
- [7] A. Alu and N. Engheta, Phys. Rev. E **95** 016623 (2005).
- [8] U. Leonhardt, Science **312** 1777-1780 (2006).
- [9] J.B. Pendry, D. Shurig, D.R. Smith, Science **312**, 1780-1782 (2006).
- [10] D. Schurig, J.J. Mock, B.J. Justice, S.A. Cummer, J.B. Pendry, A.F. Starr, D.R. Smith, Science **314**, 977-980 (2006).
- [11] F. Zolla, S. Guenneau, A. Nicolet, J.B. Pendry, Opt. Lett. **32**, 1069-1071 (2007).
- [12] A. Diatta, S. Guenneau, A. Nicolet and F. Zolla, Optics Express **17**, 13389 - 13394 (2009).
- [13] A. Greenleaf, M. Lassas and G. Uhlmann, Math. Res. Lett. **10**, 685-693 (2003).
- [14] R.V. Kohn, H. Shen, M.S. Vogelius, and M.I. Weinstein, Inverse Problems **24**, 015016 (2008).
- [15] R. Weder, Journal of Physics A: Mathematical and Theoretical **41**, 065207 (2008).
- [16] R. Weder, Journal of Physics A: Mathematical and Theoretical **41**, 415401 (2008).



- [17] D. Torrent and J. Sanchez-Dehesa, *New J. Phys.* **10**, 023004 (2008).
- [18] S.A. Cummer and D. Schurig, *New J. Phys.* **9**, 45 (2007).
- [19] F. Zolla and S. Guenneau, *Phys. Rev. E* **67**, 026610 (2003).
- [20] S.A. Cummer, B.I. Popa, D. Schurig, D.R. Smith, J. Pendry, M. Rahm, and A. Starr, *Phys. Rev. Lett.* **100**, 024301 (2008).
- [21] H. Chen and C. T. Chan, *Appl. Phys. Lett.* **91**, 183518 (2007).
- [22] M. Farhat, S. Guenneau, S. Enoch, A.B. Movchan, F. Zolla and A. Nicolet, *New J. Phys.* **10**, 115030 (2008).
- [23] M. Farhat, S. Enoch, S. Guenneau and A.B. Movchan, *Phys. Rev. B* **79**, 033102 (2009).
- [24] M. Farhat, S. Guenneau and S. Enoch, *Phys. Rev. Lett.* **103**, 024301 (2009).
- [25] M. Brun, S. Guenneau and A.B. Movchan, *Appl. Phys. Lett.* **94**, 061903, 2009 (2009).
- [26] G.W. Milton, M. Briane, and J.R. Willis, *New J. Phys.* **8**, 248 (2006).
- [27] A.N. Norris, *Proc. Roy. Soc. Lond. A* **464**, 2411 (2008).
- [28] D. Bigoni, S.K. Serkov, M. Valentini and A.B. Movchan, *Int. J. Solids Structures* **35**, 3239 (1998).
- [29] T. Chou, *Phys. Rev. Lett.* **79**, 4802 (1997).
- [30] T. Chou, *J. Fluid. Mech.* **369**, 333 (1998).
- [31] P. McIver, *J. Fluid. Mech.* **424**, 101 (2000).
- [32] M. Torres, J.P. Adrados, F.R. Montero de Espinosa, D. Garcia-Pablos, and J. Fayos, *Phys. Rev. E* **63**, 011204 (2000).
- [33] X. Hu, Y. Shen, X. Liu, R. Fu, J. Zi, X. Jiang, and S. Feng, *Phys. Rev. E* **68**, 037301 (2003).
- [34] L. Feng, X.P. Liu, M.H. Lu, Y.B. Chen, Y.F. Chen, Y.W. Mao, J. Zi, Y.Y. Zhu, S.N. Zhu and N.B. Ming, *Phys. Rev. B* **73**, 193101 (2006).

- [35] M. Farhat, S. Guenneau, S. Enoch, G. Tayeb, A.B. Movchan, N.V. Movchan, Phys. Rev. E 77, 046308 (2008).
- [36] S. Zhang, L. Yin, N. Fang, Phys. Rev. Lett. 102, 194301 (2009).
- [37] A. Sukhovich, L. Jing, J.H. Page, Phys. Rev. B 77 014301 (2008).
- [38] M. Farhat, S. Enoch, S. Guenneau and A.B. Movchan, Phys. Rev. Lett. 101, 134501 (2008).
- [39] Li, J. and Pendry, J.B., Phys. Rev. Lett. 101, 203901 (2008).
- [40] R. Liu, C. Ji, J.J. Mock, J.Y. Chin, T.J. Cui and D.R. Smith, Science **323**, 366 (2008).
- [41] L.H. Gabrielli, J. Cardenas, C.B. Poitras and M. Lipson, Nature Photonics **3**, 461-463 (2009)
- [42] J.B. Pendry and J. Li, New J. Physics 10, 115032 (2008).
- [43] E. Kallos, C. Argyropoulos and Y. Hao, Phys. Rev. A 79, 063825 (2009).
- [44] N.A.P. Nicorovici, R.C. McPhedran, S. Enoch and G. Tayeb, New J. Phys. **10**, 115020 (2008).
- [45] Y. Lai, H. Chen, Z.Q. Zhang and C.T. Chan, Phys. Rev. Lett. **102**, 093901 (2009).
- [46] A. Nicolet, F. Zolla and C. Geuzaine, (arXiv:0909.0848v1)
- [47] I.I. Smolyaninov, V.N. Smolyaninova, A.V. Kildishev and V.M. Shalaev Phys. Rev. Lett. 102, 213901 (2009)